Available online at www.sciencedirect.com
ScienceDirect
Journal of Bionic Engineering 14 (2017) 348–355

Design, Analysis and Experimental Performance of a Bionic Piezoelectric Rotary Actuator

Shupeng Wang, Weibin Rong, Lefeng Wang, Zhichao Pei, Lining Sun

State Key Laboratory of Robotics and System, *Harbin Institute of Technology*, *Harbin* 150080, *China*

Abstract

This study presents a piezoelectric rotary actuator which is equipped with a bionic driving mechanism imitating the centipede foot. The configuration and the operational principle are introduced in detail. The movement model is established to analyze the motion of the actuator. We establish a set of experimental system and corresponding experiments are conducted to evaluate the characteristics of the prototype. The results indicate that the prototype can be operated stably step by step and all steps have high reproducibility. The driving resolutions in forward and backward motions are 2.31 μrad and 1.83 μrad, respectively. The prototype can also output a relatively accurate circular motion and the maximum output torques in forward and backward directions are 76.4 Nmm and 70.6 Nmm, respectively. Under driving frequency of 1 Hz, the maximum angular velocities in forward and backward directions are 1029.3 μrad·s^{-1} and 1165 μrad·s^{-1} when the driving voltage is 120 V. Under driving voltage of 60 V, the angular velocities in forward and backward motions can be up to 235100 μrad·s^{-1} and 153650 μrad·s^{-1} when the driving frequency is 1024 Hz. We can obtain the satisfactory angular velocity by choosing a proper driving voltage and frequency for the actuator.

Keywords: bionic foot, piezoelectric rotary actuator, centipede foot, stick-slip

doi: 10.1016/S1672-6529(16)60403-1

1 Introduction

Many aspects of modern industry and technology are dependent upon ultraprecision positioning. Ultraprecision actuators are essential for semiconductor manufacture, precision optics alignment, MEMS, precision machining, and aerospace technology, *etc*. It is not uncommon that an ultraprecision actuator is required to deliver nanometer level resolution while maintaining other characteristics such as force capacity, speed, high stiffness, and adequate motion range[1–7].

Piezoelectric actuators commonly attract broad attention due to their great advantages such as small size, high resolution, large output force, rapid response and so on[7–10]. Many kinds of piezoelectric actuators have been developed by researchers all over the world. According to the working principle, piezoelectric actuators can mainly be divided into direct driving actuators, inchworm actuators, ultrasonic actuators, stick-slip actuators and so on[11–25]. Each type has its own advantages and drawbacks.

Direct driving actuators are with large force capacity and high positioning resolution, but their working range is limited[11–13]. The working range of inchworm actuators is adequate, however they usually have the drawbacks of complex flexure hinge structures and complex time-sequence signals control[14–16]. Ultrasonic actuators are with high speed motions, but wear and heat generation are still the problems[17,18]. Stick-slip actuators' main advantages are the simplification in design and stable working characteristics which offer a theoretically unlimited smooth motion with a high resolution[19–21]. Nevertheless, the traditional stick-slip actuators still have weak output forces[19–25].

As shown in Fig. 1, a centipede has dozens to hundreds feet and the feet are arc-shaped[26]. Learning from natural centipede, we design a piezoelectric rotary actuator based on bionic foot driving. In terms of the operational principle, the proposed actuator is a kind of stick-slip one. Actually it differs from traditional stick-slip actuators. The bionic foot can help the actuator produce smoother motions accompanying with larger

Corresponding author: Weibin Rong
E-mail: rwb@hit.edu.cn

output torques and higher driving resolutions.

2 Structure and moving principle

2.1 Structure of the actuator

As shown in Fig. 2, the model of the proposed actuator with specific dimensions of 100 mm × 35 mm × 17 mm mainly consists of a piezo-stack, a base, a stator, a rotor, a spindle, an adjusting bolt and a preload unit. Fig. 3 illustrates that a bionic foot, a set of guiding flexure hinges and a piezo-stack installing groove constitute the stator. The adjusting bolt is utilized to preload the piezo-stack and adjust the contact force between the tip of the bionic foot and the rotor. Fig. 4 shows that two sets of flexure hinges and two contact points constitute the preload unit, which is used to hold the position of the rotor during low driving voltage. The material of the stator and the preload unit is 65 Mn in order to obtain good elastic properties of the bionic foot and the flexure hinges.

2.2 Moving principle

Fig. 5 illustrates that a sawtooth-wave voltage is applied to the piezo-stack and the working process of the designed actuator is divided into three stages as follows.

Initially, as shown in Fig. 5a, at t_0, the piezo-stack without voltage applied to is at its natural length. The rotor can be held by two contact points of the preload unit and the tip of the bionic foot. There is a suitable contact force between the tip of the bionic foot and the rotor and the contact force can be adjusted by the adjusting bolt.

Secondly, as shown in Fig. 5b, from t_0 to t_1, the piezo-stack gets expanded slowly to its maximum position as a result of slow increase in the applied voltage, during which the bionic foot bends and rotates the rotor in anticlockwise direction by a small angle α_1 (the first angular displacement).

Thirdly, as shown in Fig. 5c, from t_1 to t_2, the piezo-stack contracts quickly to its initial position as a result of quick decrease in the applied voltage, during which the bionic foot also returns to its free shape momentarily due to the elastic properties. Meanwhile, the rotor rotates back by a small angle α_2 (the second angular displacement) under the actions of its own inertia and the friction forces from the tip of the bionic foot and contact points of the preload unit. In consequence, the rotor rotates one step in anticlockwise direction and the step angle can be calculated,

$$\alpha=\alpha_1-\alpha_2. \tag{1}$$

At this time, the actuator restores to its initial state again.

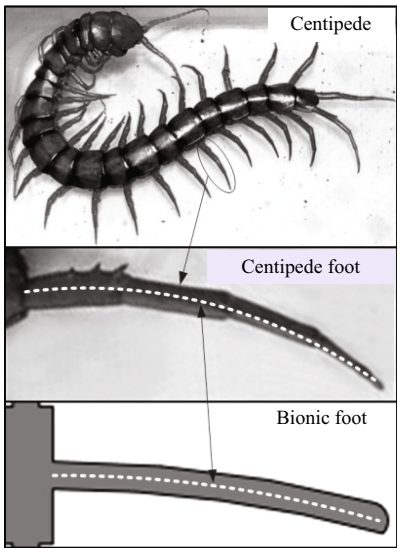

Fig. 1 Centipede and bionic foot.

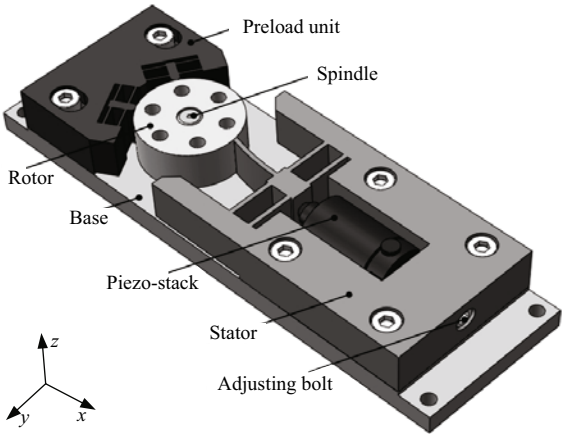

Fig. 2 Model of the actuator.

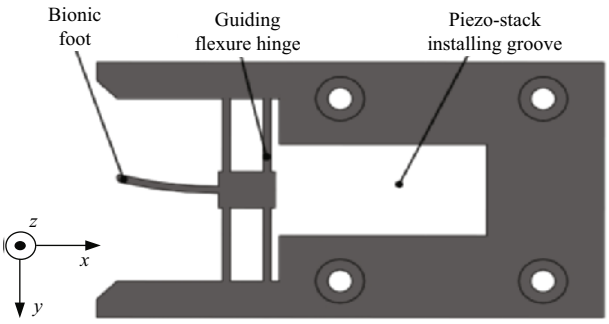

Fig. 3 Structure of the stator.

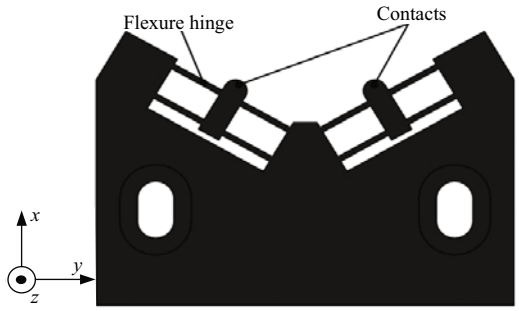

Fig. 4 Structure of the preload unit.

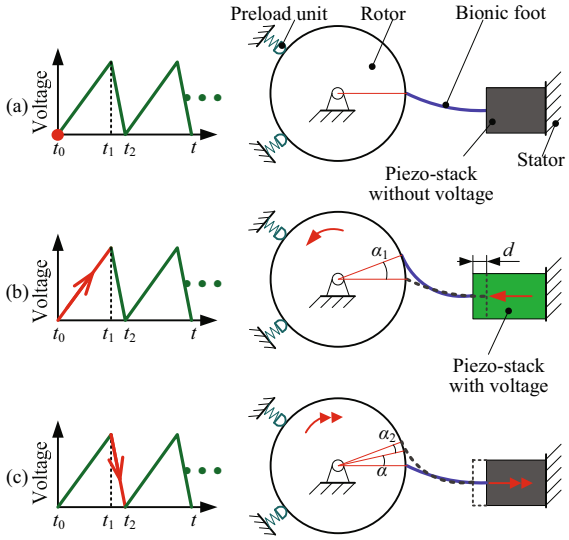

Fig. 5 Working process of the actuator. (a) Initial state; (b) the piezo-stack extends slowly; (c) the piezo-stack contracts quickly.

After the three stages, one working circle of the proposed actuator is completed. By repeating the stages (a) to (c), the actuator can output an unlimited range rotary motion step by step. Furthermore, the backward motion can be obtained by changing the direction of the sawtooth-wave voltage applied to the piezo-stack.

3 Analysis

As shown in Fig. 6, the movement model of the actuator is established. A rotation pair is used to simulate the contact between the tip of the bionic foot and the rotor at point *C*. The force analysis of the bionic foot is conducted in Fig. 7 and it shows that the force situation of the bionic foot (Fig. 7a) is equivalent to the situation shown in Fig. 7b. According to Ref. [21], the displacements of point *C* in *x* and *y* directions can be obtained from the following equations,

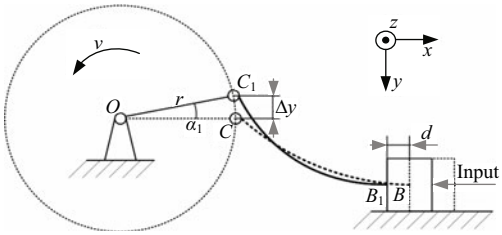

Fig. 6 Movement model of the actuator.

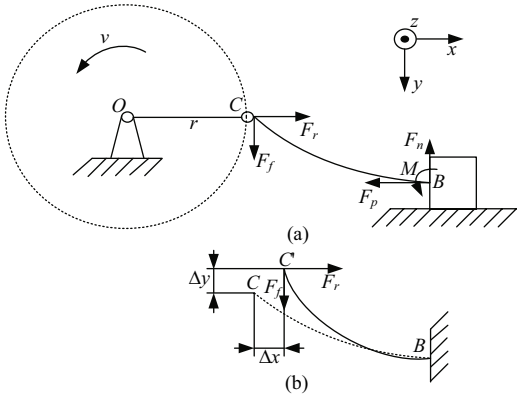

Fig. 7 Force analysis of the bionic foot. (a) Force situation of the bionic foot; (b) force analysis.

$$\Delta x = -\frac{F_f R^3}{2EI}\left(2\cos^2\theta + 2\theta\sin\theta\cos\theta - 2\cos\theta - \sin^2\theta\right) - \frac{F_r R^3}{2EI}\left(2\theta\cos^2\theta - 3\sin\theta\cos\theta + \theta\right) - \frac{F_f R}{2EA}\sin^2\theta - \frac{F_r R}{2EA}\left(\theta + \sin\theta\cos\theta\right), \tag{2}$$

$$\Delta y = \frac{F_f R^3}{2EI}\left(2\theta\sin^2\theta + 3\sin\theta\cos\theta - 4\sin\theta + \theta\right) + \frac{F_r R^3}{2EI}\left(\cos^2\theta + 2\theta\sin\theta\cos\theta - 2\cos\theta - 2\sin^2\theta + 1\right) + \frac{F_f R}{2EA}\left(\theta - \sin\theta\cos\theta\right) + \frac{F_r R}{2EA}\sin^2\theta, \tag{3}$$

where R and θ are the curvature radius and the central angle of the bionic foot curve, I is the moment of inertia, A is the area of cross section, E is the elastic modulus of the material. F_f is the sum of the initial friction and the external load, F_r is equal to horizontal thrust of the bionic foot base (point *B*).

Since the deformation of the bionic foot is very small, the deformation (Δx) in *x* direction can be approximated to the elongation (d) of the piezo-stack. So the following equation can be got,

$$\Delta y = d\left[\begin{array}{l}\dfrac{F_f R^3}{2EI}\left(2\theta\sin^2\theta+3\sin\theta\cos\theta-4\sin\theta+\theta\right)+\\ \dfrac{F_r R^3}{2EI}\left(\cos^2\theta+2\theta\sin\theta\cos\theta-2\cos\theta-2\sin^2\theta+1\right)\\ +\dfrac{F_f R}{2EA}\left(\theta-\sin\theta\cos\theta\right)+\dfrac{F_r R}{2EA}\sin^2\theta\end{array}\right] \Big/ \left[\begin{array}{l}-\dfrac{F_f R^3}{2EI}\left(2\cos^2\theta+2\theta\sin\theta\cos\theta-2\cos\theta-\sin^2\theta\right)\\ -\dfrac{F_r R^3}{2EI}\left(2\theta\cos^2\theta-3\sin\theta\cos\theta+\theta\right)-\\ \dfrac{F_f R}{2EA}\sin^2\theta-\dfrac{F_r R}{2EA}\left(\theta+\sin\theta\cos\theta\right)\end{array}\right] \tag{4}$$

The first angular displacement α_1 can be calculated by the following equation:

$$\alpha_1 \approx \Delta y / r$$

$$= \frac{d}{r}\left[\begin{array}{l}\dfrac{F_f R^2}{I}\left(2\theta\sin^2\theta+3\sin\theta\cos\theta-4\sin\theta+\theta\right)+\\ \dfrac{F_r R^2}{I}\left(\cos^2\theta+2\theta\sin\theta\cos\theta-2\cos\theta-2\sin^2\theta+1\right)\\ +\dfrac{F_f}{A}\left(\theta-\sin\theta\cos\theta\right)+\dfrac{F_r}{A}\sin^2\theta\end{array}\right] \Big/ \left[\begin{array}{l}-\dfrac{F_f R^2}{I}\left(2\cos^2\theta+2\theta\sin\theta\cos\theta-2\cos\theta-\sin^2\theta\right)\\ -\dfrac{F_r R^2}{I}\left(2\theta\cos^2\theta-3\sin\theta\cos\theta+\theta\right)-\\ \dfrac{F_f}{A}\sin^2\theta-\dfrac{F_r}{A}\left(\theta+\sin\theta\cos\theta\right)\end{array}\right]. \tag{5}$$

4 Experiments

In order to study the characteristics of the bionic actuator, we establish a set of experimental system which consists of an Industry Personal Computer (IPC), a capacitance micrometer, a signal generator, a signal amplifier, and the actuator prototype. As shown in Fig. 8, the original voltage signal is produced and enlarged by the signal generator and the signal amplifier and then it is applied to the piezo-stack to drive the actuator prototype. In the meantime the capacitance micrometer measures the distance changes between the capacitive sensor and the reflector which is fixed on the rotor. Finally, all the data is gathered and processed by the IPC.

4.1 Output under various driving voltages

Fig. 9 shows the forward and backward output curves of the actuator prototype under various driving voltages when the driving frequency is 1 Hz. It can be observed that the actuator operates stably step by step under every voltage and all steps have high reproducibility. This indicates that at every step of the motions, both the first angular displacement α_1 and the second angular displacement α_2 which are analyzed in section **2.2** are in a good operation state. There is a significant positive correlation between the slopes of the output curves and the driving voltages in both the forward and backward motions. The maximum step angles can be up to 1029.3 μrad in forward motion and 1165 μrad in backward motion under driving voltage of 120 V. As shown in Fig. 9, a satisfactory step angle can be obtained if we choose a proper driving voltage for the actuator.

4.2 Driving resolution

Driving resolution is a significant performance parameter for an actuator and it is refer to the minimum stable step angle for a rotary actuator. According to

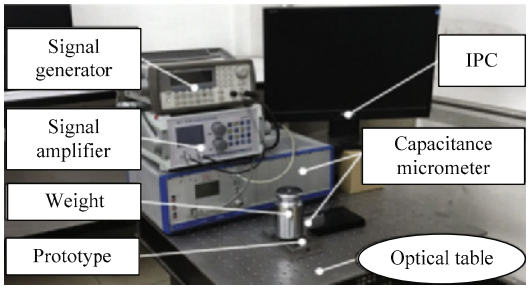

Fig. 8 The established experimental system.

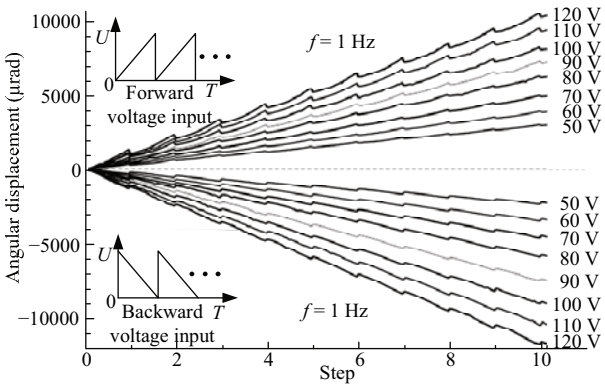

Fig. 9 Outputs under various driving voltages.

section **4.1**, the step angle gradually reduces with the decrease in driving voltage. So we can obtain the drivingresolution of the actuator prototype by continuously reducing the driving voltage. After a great deal of experiments, it can be concluded that the prototype cannot run stably in forward direction if the driving voltage is below 13 V and in backward direction if the driving voltage is below 11 V. This may be because that there is clearance between the rotor and the spindle.

As shown in Fig. 10, a final angular displacement by 100 steps in forward direction is recorded as about 230.8 μrad. Hence, the average step angle is about 2.31 μrad, which can be regarded as the driving resolution of the actuator prototype in forward motion. Similarly, another final angular displacement by 100 steps in backward direction is about 182.6 μrad. So the driving resolution of the prototype in backward motion is about 1.83 μrad.

4.3 Output under various driving frequencies

Fig. 11 shows the good linear relationships between the angular displacement and time under various driving frequencies with a constant driving voltage of 60 V in both forward and backward motions. We can found that the actuator runs stably step by step under every frequency and all steps have high reproducibility. This also indicates that at every step of the motions under every frequency, both the first angular displacement α_1 and the second angular displacement α_2 are in a good operation state. With the increase in driving frequency, the slopes of the curves gradually increase. That means that the rotation velocity of the actuator prototype increases. Similarly, we can obtain a satisfactory angular velocity by choosing a proper driving frequency for the actuator.

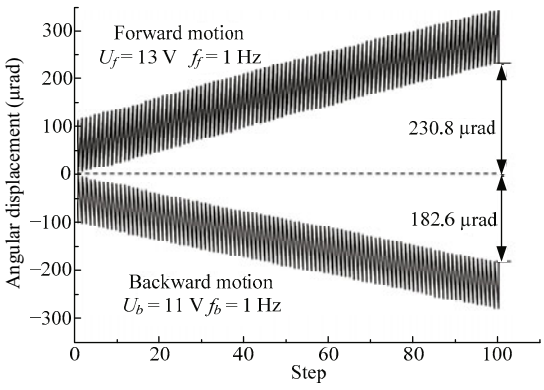

Fig. 10 Output curves in resolution test.

4.4 Motion velocity

Driving voltage and frequency are two important parameters to determine the motion velocity of the developed actuator. In order to study the motion velocity, a large number of tests (no-load condition) are conducted under various driving voltages and frequencies in both forward and backward directions.

Fig. 12 gives the good linear relationship between the angular velocity and driving voltage under a constant working frequency of 1 Hz. It can be observed that with the increase in driving voltages, the angular velocity of the actuator prototype increases and the backward velocity is more sensitive to the changes of driving voltage. Under the driving frequency of 1 Hz, the maximum angular velocities in forward and backward directions are 1029.3 μrad·s^{-1} and 1165 μrad·s^{-1}, respectively.

The relationship between the angular velocity and working frequency is shown in Fig. 13. We can find that with the increase in driving frequencies, the angular velocity of the actuator prototype also increases. Under the driving voltage of 60 V, the angular velocities in forward

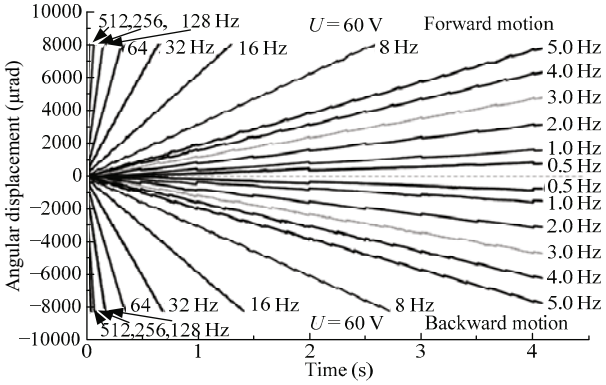

Fig. 11 Outputs under various driving frequencies.

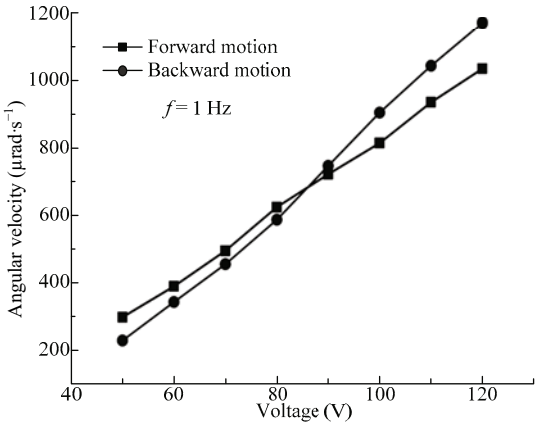

Fig. 12 Angular velocities under various driving voltages.

and backward motions can be up to 235100 μrad·s^{-1} and 153650 μrad·s^{-1} when the driving frequency is 1024 Hz. There are good linear relationships between the velocity and driving frequency in both forward and backward directions when the frequency is below 256 Hz. However, the angular velocity is gradually saturated while the driving frequency exceeds 256 Hz. This may be because of the low response speed of the mechanical structure. The response speeds of the flexure hinges cannot follow with the driving signals under high frequency.

4.5 Circular motion

As mentioned in section **2.2**, the actuator can output an unlimited range rotary motion step by step. In order to test the circular motion, a mark point is painted atop the rotor as a reference and its trajectory is monitored by a high speed video camera. Transient position of the reference is tracked by image processing method to get its coordinates, which are then plotted by blue points in Fig. 14 to show the trajectory of the reference. The least-squares fit method is then adopted to find out the parameters of the assumed circular trajectory, including its radius and center, as shown in Fig. 14 with red circle and red point, respectively. The experimental results indicate that the measured trajectory is a fine circle, which confirms that the designed actuator can output a relatively accurate circular motion.

4.6 Output torque

In order to test the output torque of the actuator prototype, a lever is fixed on the rotor and Fig. 15 shows the working schematic of the experimental system. The thread is used to tow the weight and the arm of the force is 20 mm. After a large number of experiments, the negative correlation relationships between the step angle and torque are presented in Fig. 16. The graph indicates that the step angle of the actuator decreases with the increase in torque in both forward and backward motions.

When the applied weight is larger than 390 g in forward motion and 360 g in backward motion, the designed actuator cannot work smoothly. Hence the output torques of the actuator prototype in forward and backward motions are 76.4 Nmm and 70.6 Nmm, respectively.

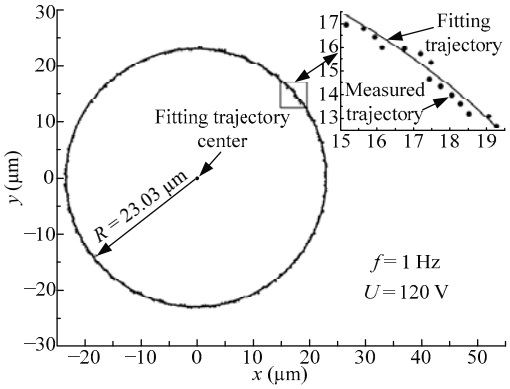

Fig. 14 Circular motion trajectory.

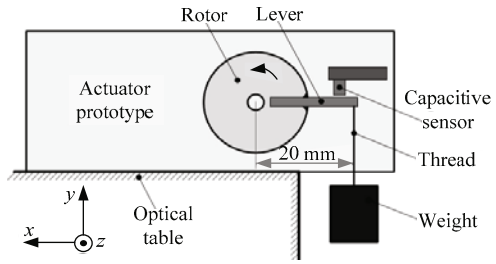

Fig. 15 Torque outputs experimental system.

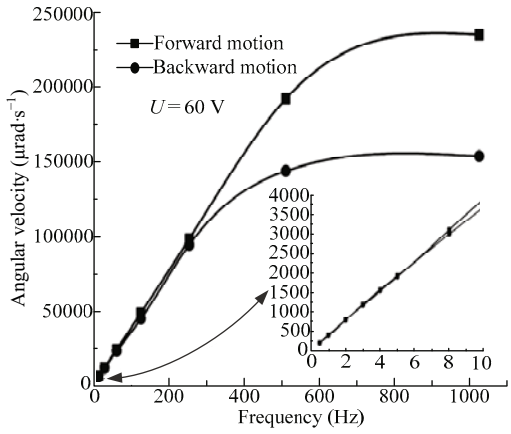

Fig. 13 Angular velocities under various driving frequencies.

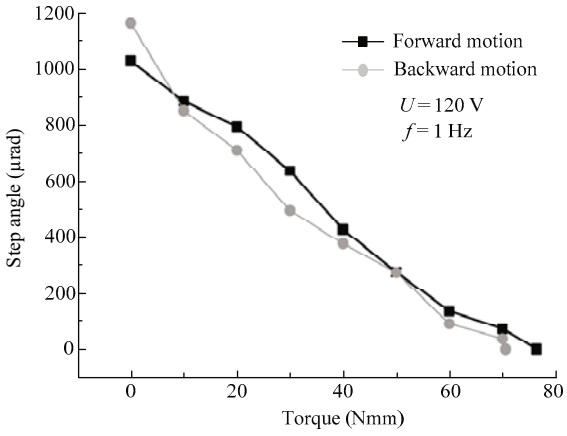

Fig. 16 Step angles under various torques.

5 Conclusion

A piezoelectric rotary actuator based on bionic foot driving is proposed in this paper. The actuator is equipped with a bionic driving mechanism imitating the centipede foot. The mechanical structure and key components are illustrated and the working principle of the actuator is introduced in detail. We also establish the movement model to analyze the motion of the actuator. An experimental system is set up and corresponding experiments are conducted to evaluate the performance of the fabricated prototype. The experimental results indicate that the prototype can operate stably step by step under various driving voltages and frequencies and all steps have high reproducibility. The driving resolutions in forward and backward motions are 2.31 μrad and 1.83 μrad, respectively. The prototype can also output a relatively accurate circular motion and the maximum output torques in forward and backward motions are 76.4 Nmm and 70.6 Nmm, respectively. Under driving frequency of 1 Hz, the maximum angular velocities in forward and backward directions are 1029.3 μrad·s^{-1} and 1165μrad·s^{-1} when the driving voltage is 120 V. Under driving voltage of 60 V, the angular velocities in forward and backward motions can be up to 235100 μrad·s^{-1} and 153650 μrad·s^{-1} when the driving frequency is 1024 Hz. We can obtain a satisfactory angular velocity by choosing a proper driving voltage and frequency for the actuator.

In summary, this research indicates that the proposed actuator based on bionic foot driving can satisfy the requirements for precise motion with high resolution and large loading capacity. Future works will be taken to optimize the geometric parameters of the bionic foot so that the actuator can achieve better performance.

Acknowledgment

This research is funded by the National Natural Science Foundation of China (No. 51675141) and the Foundation for Innovative Research Groups of the National Natural Science Foundation of China (No. 51521003).

References

[1] Awaddy B A, Shih W C, Auslander D M. Nanometer positioning of a linear motion stage under static loads. *IEEE/ASME Transactions on Mechatronics*, 1998, **3**, 113–119.

[2] Tenzer P E, Mrad R B. A systematic procedure for the design of piezoelectric inchworm precision positioners. *IEEE/ASME Transactions on Mechatronics*, 2004, **9**, 427–435.

[3] Li J, Zhou X, Zhao H, Shao M, Hou P, Xu X. Design and experimental performances of a piezoelectric linear actuator by means of lateral motion. *Smart Materials and Structures*, 2015, **24**, 065007.

[4] Heo S, Wiguna T, Park H C, Goo N S. Effect of an artificial caudal fin on the performance of a biomimetic fish robot propelled by piezoelectric actuators. *Journal of Bionic Engineering*, 2007, **4**, 151–158.

[5] Liu W T, Zhou M Y, Stefanini C, Fu X. Modeling and preliminary analysis of a miniaturized rotary motor driven by single piezoelectric stack actuator. *Journal of Intelligent Material Systems and Structures*, 2016, **27**, doi: 1045389X15595293.

[6] Ho T, Lee S. Piezoelectrically actuated biomimetic self-contained quadruped bounding robot. *Journal of Bionic Engineering*, 2009, **6**, 29–36.

[7] Ho S T, Jan S J. A piezoelectric motor for precision positioning applications. *Precision Engineering*, 2016, **43**, 285–293.

[8] Peng Y X, Cao J, Liu L, Yu H Y. A piezo-driven flapping wing mechanism for micro air vehicles. *Microsystem Technologies*, 2017, 23, 967–973.

[9] Yong Y K, Moheimani S R, Kenton B J, Leang K K. Invited review article: High-speed flexure-guided nanopositioning: Mechanical design and control issues. *Review of Scientific Instruments*, 2012, **83**, 121101.

[10] Wang S, Zhang Z, Ren L, Zhao H, Liang Y, Zhu B. Design and driving characteristics of a novel “pusher” type piezoelectric actuator. *Smart Materials and Structures*, 2015, **25**, 015005.

[11] Tian Y, Zhang D, Shirinzadeh B. Dynamic modelling of a flexure-based mechanism for ultra-precision grinding operation. *Precision Engineering*, 2011, **35**, 554–565.

[12] Gu G Y, Zhu L M, Su C Y. High-precision control of piezoelectric nanopositioning stages using hysteresis compensator and disturbance observer. *Smart Materials and Structures*, 2014, **23**, 105007.

[13] Yao Q, Dong J, Ferreira P M. Design, analysis, fabrication and testing of a parallel-kinematic micropositioning XY stage. *International Journal of Machine Tools and Manufacture*, 2007, **47**, 946–961.

[14] Bexell M, Johansson S. Fabrication and evaluation of a piezoelectric miniature motor. *Sensors and Actuators A*:

Physical, 1999, **75**, 8–16.

[15] Drevniok B, Paul W M P, Hairsine K R, McLean A B. Methods and instrumentation for piezoelectric motors. *Review of Scientific Instruments*, 2012, **83**, 033706.

[16] Zhang Z M, An Q, Li J W, Zhang W J. Piezoelectric friction–inertia actuator-a critical review and future perspective. *The International Journal of Advanced Manufacturing Technology*, 2012, **62**, 669–685.

[17] Shi Y, Zhao C. A new standing-wave-type linear ultrasonic motor based on in-plane modes. *Ultrasonics*, 2011, **51**, 397–404.

[18] Liu Y, Chen W, Liu J, Shi S. Actuating mechanism and design of a cylindrical traveling wave ultrasonic motor using cantilever type composite transducer. *PlOS ONE*, 2010, **5**, e10020.

[19] Neuman J, Nováček Z, Pavera M, Zlámal J, Kalousek R, Spousta, J, Dittrichová L, Šikola, T. Experimental optimization of power-function-shaped drive pulse for stick-slip piezo actuators. *Precision Engineering*, 2015, **42**, 187–194.

[20] Nguyen H X, Edeler C, Fatikow S. Contact mechanics modeling of piezo-actuated stick-slip microdrives. *Physical Mesomechanics*, 2012, **15**, 280–286.

[21] Wang S, Rong W, Wang L, Sun L. Design, analysis and experimental performance of a stepping type piezoelectric linear actuator based on compliant foot driving. *Smart Materials and Structures*, 2016, **25**, 115003.

[22] Edeler C, Meyer I, Fatikow S. Modeling of stick-slip micro-drives. *Journal of Micro-Nano Mechatronics*, 2011, **6**, 65–87.

[23] Peng Y, Wang H, Wang S, Wang J, Cao J, Yu H. Design and experimental validation of a linear piezoelectric micromotor for dual-slider positioning. *Microsystem Technologies*, 2016, 1–8.

[24] Hunstig M, Hemsel T, Sextro W. Stick-slip and slip-slip operation of piezoelectric inertia drives. Part I: Ideal excitation. *Sensors and Actuators A*: *Physical*, 2013, **200**, 90–100.

[25] Edeler C, Fatikow S. Open loop force control of piezo-actuated stick-slip drives. *International Journal of Intelligent Mechatronics* & *Robotics*, 2013, **1**, 1–19.

[26] Masuda M, Ito K. Semi-autonomous centipede-like robot with flexible legs. *IEEE International Symposium on Safety*, *Security*, *and Rescue Robotics*, Hokkaido, Japan, 2014, 1–6.